**UNIVERSIDAD DE LAS PALMAS DE GRAN CANARIA**

**Facultad de Ciencias del Mar**

**Departamento de Física**

---

*Proyecto Final de Máster – Tesina:*

# Towards the construction of a validated numerical system to study the mesoscale dynamics of the North-East Atlantic (2003-2006) case study.

*Sheila Natalí Estrada-Allis*

Director: Ángel Rodríguez Santana

Co-directores: Rui Caldeira Andrade y Pablo Sangrà Inciarte

*Las Palmas de Gran Canaria a 3 de Febrero de 2011*

# Towards the construction of a validated numerical system to study the mesoscale dynamics of the North East Atlantic (2003-2006)

S.N. Estrada-Allis[a,c], X. Couvelard[b], R.M. Caldeira[b,c,1,*], F. Machín[a], A. Rodríguez-Santana[a], P. Sangrà[a]

[a] *Departamento de Física. Facultad de Ciencias del Mar. Universidad de Las Palmas de Gran Canaria (ULPGC). Las Palmas. Spain*
[b] *Center for Mathematical Sciences (CCM) University of Madeira. Madeira Island. Portugal*
[c] *Interdisciplinary Centre of Marine and Environmental Research (CIIMAR). Porto. Portugal*

**Abstract**

A detailed validation study has contributed to the construction of a NE-Atlantic (NEA), ocean circulation model, for the 2003-2006 period. The comparisons between three model solutions, remote sensing and in situ data, focused on the study of the most dynamical processes of NEA sub-regions. Model validations include (i) comparisons with Sea Surface Temperature (SST), from AVHRR and Microwave-OI; (ii) Eddy Kinetic Energy (EKE), computed from altimetry; (iii) Temperature and Salinity profiles computed from ARGO floats, and (iv) sub-surface temperature, measured in three buoys of 'Puertos del Estado'. Simple statistical methods were used to quantify model-data comparisons. In general, model regional solutions show a

*Corresponding author
*Email address:* rcaldeira@ciimar.up.pt (R.M. Caldeira)
[1] CIIMAR, Rua dos Bragas, 289, 4050-123 Porto, Portugal, Ph (+351) 22 340 18 00, Fax (+351) 22 339 06 08

good correlation and small Root Mean Squared Error (RMSE) with SST and EKE. The main water masses were well depicted by the regional model; while the region with high salinity values, often dominated by Mediterranean Intermediate Water (MIW), was not accurately resolved. The initial condition and boundary forcing of the regional model was evaluated, particularly concerning the usage of Ocean General Circulation Models (OGCM's), as an alternative to the classical climatological forcing. The analysis of their Kolmogorov energy spectrum determined their effective resolutions and their EKE levels. Mercator global solution at 1/4°, was shown to be an adequate OGCM solution for studying the 2003-2006 period. The energy spectrum analysis also showed that new 1/12° (downscaled), regional solution resolved more energetic scales than the original OGCM, confirming the need to use high spatial resolution regional ocean circulation models to resolve mesoscale and sub-mesoscale phenomena. The regional model (ROMS) was able to reproduce an Iberian Peninsula upwelling event as well as other previously documented NEA processes, such as the westward propagating eddies associated with the Azores Front, with the Canary and with Madeira Archipelagos. The analysis also showed that atmospheric forcing, is important to adequately resolve surface dynamics. However, other more conservative aspects of the ocean such as the water mass composition, are better represented with climatological forcing.

*Keywords:*

ROMS, North Eastern Atlantic, model validation, atmospheric-ocean interactions, boundary conditions.

---

## 1. Introduction

The North East Atlantic ocean (NEA) is a very dynamic oceanic region with identifiable sub-systems; these sub-systems can be considered as "critical regions", characterized by the high values of eddy kinetic energy (EKE), (Fig. 1). The main critical regions of the NEA, identified using altimetry derived data for their high EKE activity (Fig. 1), are: (i).- Iberian Peninsula (IP); (ii).- The Mediterranean Water Outflow (MWO); (iii).- The Azores Front region (AF); (iv).- Madeira Archipelago (MA); (v).- Canaries Archipelago (CA) and (vi).- The Azores Archipelago (AA).

The IP sub-region is part of the four main driven eastern boundary upwelling zones, hereafter refer to as IPUS (Iberian Peninsula Upwelling System), with a strong seasonal variability (e.g. Alvarez et al., 2009). Two water masses play an important role: (i) the Mediterranean Intermediate Water (MIW), since the upwelling is in the pathway of anticyclonic mesoscale lens of warm salty of Mediterranean Water (Meddies) (e.g. Armi and Stommel, 1983; Relvas et al., 2007); (ii) the Eastern North Atlantic Central Water (ENACW), that is, in general, observed in upwelled waters (e.g. Pollard et al., 1996). In absence of coastal upwelling, the surface circulation off Western Iberia is predominantly poleward (e.g. Peliz et al., 2002). Another important and recurrent structure in the IPUS are the upwelling filaments (e.g. Barton et al., 2001), as well as the long trapped filaments (see Meunier et al., 2010). Satellite data (Haynes et al., 1993) and models results (Haidvogel et al., 1991) show that large filaments are often closely related with the location of capes and promontories.

Laboratory studies by Mauritzen et al. (2001) hypothesize that the MWO

Mediterranean Water Outflow exerts a strong influence in the North East Atlantic dynamics. Downstream of the Gibraltar Strait, higher salinities were measured in the surface waters of the Gulf of Cadiz, through a detrainment process (i.e. due to diapycnal mixing of flux of salinity from the MWO towards the low-density Central Water). The surface waters travel westward and northward, promoting the salinity increase in the Central Water off the West IP (see Relvas et al., 2007). Furthermore, previous modeling studies suggest the existence of a direct link between the Azores Current and the MWO (e.g. Relvas et al., 2007; Volkov and Fu, 2010). The formation of the well-defined zonally oriented Azores Current may be the result of water mass transformation associated with MWO in the Gulf of Cadiz (Volkov and Fu, 2010).

The Azores Current, and its associated front (AF), is a quasi-permanent NEA feature throughout the year, centered between 33° and 35 °N (e.g. Klein and Siedler, 1989). The complex mesoscale variability of the AF is characterized by long periods ($\sim$ 250 days) and large wavelengths ($\sim$ 600km), with westward propagation, associated with Rossby waves (Le Traon and De Mey, 1994) and are largely due to baroclinic instabilities (e.g. Alves and De Verdière, 1999). Chelton et al. (2007), also suggested that the westward energy propagation at mid-latitudes is more representative of nonlinear vertically-coherent eddies, as an alternative to the Rossby wave propagation theory.

Islands are also regions with strong mesoscale activity in the NEA. Sangrà et al. (2009) reported the existence of several west propagating eddy corridors at the AF and leeward of the islands. Two small eddies corridors were

identified north and south of the AF. These west propagating cyclonic eddies were first observed at 32.2 °N from in-situ data (Pingree and Sinha, 2001) and presented as an alternative hypothesis, which had previously associated these westward propagation with the occurrence of planetary Rossby waves. Another zonal corridor was also detected at 31 °N, south of MA and south of the CA. The Canary Eddy Corridor, extending from 22 °N to 29 °N, and populated mainly by anticyclones. Both Madeira and Canary eddy corridors, had well defined source regions i.e. leeward side of the islands.

The first attempts to study the dynamical mesoscale sub-systems of the NEA, using only Ocean Global Circulation Models (OGCM), did not reproduce well the mesoscale structures often observed from in-situ and remote sensing data (e.g Pingree, 2002). Mesoscale eddies are parameterized as a viscous term playing an important role in energy and momentum dissipation in ocean circulation models, not well resolved in OGCMs (Jochum et al., 2008). Another OGCM limitation is their direct impact on deep-ocean currents, which are largely constrained by the poor representation of the oceanic bathymetry (Barth et al., 2008). Nevertheless, OGCMs can provide adequate boundary and initial conditions for high-resolution regional ocean models (Barth et al., 2008; Melsom et al., 2009; Alvera-Azcárate et al., 2011). Currently, there are several OGCM solutions freely available to the scientific community. These include: (i) Mercator, (ii) SODA, (iii) ECCO and (iv) HYCOM. In order to determine which OGCM to use, their accuracy and availability of their solutions were considered herein. Classical climatological forcing was also considered, as an alternative control experiment.

Previous studies (Mason et al., 2011) used high resolution regional models

to study some aspects of the NEA dynamics, forcing their model with climatological data. To the best of our knowledge, no previous studies evaluated the relative role of OGCMs and climatological boundary forcing, to study the NEA dynamics. Ultimately, our main goal is to construct a validated ocean regional model, considering the tools and the data available today, in order to adequately continue to investigate the regional dynamics. It is expected that this system and its validation protocols will evolve into a regional ocean forecasting system.

The layout of this report is as follows, after the introduction (section 1), Section 2 describes the different sources of data used, as well as, a detailed description of the regional numerical modeling system, the different aspects of the experiments, their boundary and initial conditions and the statistical metrics used for comparing model results with data. Section 3 discusses the main results including: (i) The representation of sub-mesoscale NEA processes; (ii) The representation of the surface dynamics; and (iii) the capability of our regional model to reproduce previously documented dynamic processes, such as the westward propagation eddies, the representation of main water masses and an IPUS episode. Section 4 sums up the results and proposes future directions.

## 2. Data sources and Methods

### *2.1. The regional ocean circulation modeling system*

The regional model used in this study was the Regional Oceanic Modeling System (ROMS). For a complete description of the model referred to (Shchepetkin and McWilliams, 2003, 2005). ROMS is a split-explicit, free-

surface and terrain-following vertical coordinate oceanic model, where short time steps are used to advance the surface elevation and barotropic momentum equation, and a larger time step is used for temperature, salinity, and baroclinic momentum. ROMS employs a two-way time-averaging procedure for the barotropic mode which satisfies the 3D continuity equation. The specially designed predictor-corrector time-step algorithm allows a substantial increase in the permissible time-step size. The third-order, upstream-biased, dissipative advection scheme for momentum allows the generation of steep gradients, enhancing the effective resolution of the solution for a given grid size Shchepetkin and Mcwilliams (1998). For tracers, the RSUP3 scheme where diffusion is split from advection and is represented by a rotated biharmonic diffusion scheme with flow-dependent hyper-diffusivity, is used in order to avoid excessive spurious diapycnal mixing associated with sigma coordinates Marchesiello et al. (2009). Explicit lateral viscosity is null everywhere in the model, except in sponge layers near the open boundaries where it increases smoothly on several grid points. A K-profile parameterization (KPP) boundary layer scheme Large et al. (1994) parameterizes the sub-grid vertical mixing processes.

In order to encompass the most relevant dynamic features of the NEA circulation, and considering the oceanographic dataset available for model validation, we have designed an extended rectangular grid from 25 °N to 45 °N in latitude and from 35 °W to 5 °W in longitude.

The model grid, forcing initial and boundary conditions are built using an adapted version of the ROMSTOOLS package (Penven, 2003). The bottom topography is derived from a 30 arc-second resolution database GEBCO_08

(www.gebco.net). Although a new pressure gradient scheme associated to a modified equation of state limits computational errors of the pressure gradient is currently implemented in ROMS (Shchepetkin and McWilliams, 2003), the bathymetry still needs to be smoothed, so that the "slope parameter" $r=\Delta h/h$ (Beckmann and Haidvogel, 1993) remains under 0.2. To preserve a sufficient resolution in the upper ocean, we use 50 vertical levels with stretched s-coordinates, using surface and bottom stretching parameters $\theta$s=6, $\theta$b=0 (Song and Haidvogel, 1994).

Three ROMS experiments were built for this study, they differed on the source and nature of their oceanic boundary conditions and on the source and nature of their atmospheric forcing conditions. These include: (1) R_M, ROMS forced with Mercator at the oceanic boundaries. Half degree, daily mean wind stress was extracted from the QuikSCAT satellite scatterometer data, provided by CERSAT (www.ifremer.fr/cersat/en/index.htm); heat and fresh water fluxes were extracted from NCEP2, using the bulk formula Fairall et al. (1996, 2003); (2) R_NQ, ROMS was forced with WOA05 climatology (Locarnini et al., 2006; Antonov et al., 2006) at the ocean boundary, momentum fluxes were extracted from QuiKSCAT and heat fluxes from NCEP2; (3) R_C, ROMS forced with WOA05 climatology at the oceanic boundaries, and COADS climatology (da Silva et al., 1994) (atmospheric heat and momentum).

The lateral boundaries facing the open ocean, a mixed passive-active, implicit, radiation condition connects the model solution to the surroundings (Marchesiello et al., 2001). Regarding the Mercator inflow conditions, the solution at the boundary is nudged toward daily time-averaged outputs, which

had been run on a 1/4° resolution grid, from 1993 to 2008 (PSY3V2). All the ROMS experiment had a 1/12° resolution (i.e. about 8 km), and were calculated in realistic mode i.e. using the full dynamical equations, thus taking advantage of our parallel computing system i.e. using 40-cpus per run. The spin-up time for all simulations is 2 years and analyses were performed for the period 2003-2006.

*2.2. Data used for model validation*

In order to evaluate the quality of the model solutions as well as to estimate model errors, several sources of data were considered (summarized in table 1). The four OGCM solutions only overlapped for the 2003-2006 period; therefore, the analysis of model performance and validations were concentrated on that period. Moreover, the Mercator product available for the NEA for the 2003-2006, did not include data assimilation, thus data used for model validation could be used independently (see e.g. Bahurel et al., 2004).

The first dataset considered was the AVISO altimetry, freely available through an OpenDAP server (http://www.aviso.oceanobs.com). The merged product of Ssalto/Duacs Gridded product produced Sea level anomalies and geostrophic velocity anomalies at a spatial resolution of 1/3° x 1/3°, and with weekly resolution. For this study, Maps of Sea Level Anomalies (MSLA), were based on the satellites: Jason-1 & 2, Topex-Poseidon, Envisat, GFO,ERS-1 & 2 and Geosat. The SLA data from AVISO was used to compute the Eddy Kinetic Energy (EKE). In order to keep consistency, both EKE extracted from altimetry and from the models were derived from SLA.

Two independent Sea Surface Temperature (SST) products were consid-

ered; (i) the SST product derived from infra-red sensor flying onboard of the AVHRR-Advanced Very High Resolution Radiometer (AVHRR hereafter); (ii) SST derived from TMI-AMSRE data from Microwave (MW_SST hereafter). Both SST products have been used to create a cloud and gap free, daily product, using optimal interpolation at a spatial grid resolution of 0.25° x 0.25° (for more details see Reynolds et al., 2007). The AVHRR product can be downloaded through the ftp site (ftp://eclipse.ncdc.noaa.gov/pub/OI-daily-v2/NetCDF/).This product uses NODCs AVHRR Pathfinder Version 5 (currently available from January 1985 through December 2005) and the operational data, available from 2006 to the present. The Pathfinder AVHRR compares well the in situ data (Reynolds et al., 2007). The final product includes a bias correction of the satellite data with respect to in situ data using an Empirical Orthogonal Teleconnection (EOT) algorithm. The EOT procedure is extensively discussed in Reynolds et al. (2007). The Microwave SST product is downloaded in binary data format, available via ftp (ftp.discover-earth.org/sst). The global AMSR-E (Advanced Microwave Scanning Radiometer-EOS) SST product, is available from June 2002 to the present. This merged data uses the OI scheme described in Reynolds and Smith (1994).

The characterization of the NEA water masses was done comparing model profiles with profiles extracted from the ARGO profiles, available from ifremer-coriolis (http://www.ifremer.fr/cgi-bin/nph-dods/data/in-situ/argo/dac/coriolis/). These floats take profiles of Temperature and Salinity, from 0 to 2000 m depth, over a 5-10 day repetitive cycle. Only the best quality controlled (QC=1), T/S profiles, from January 2003 to December 2006 were consid-

ered.

Since the ARGO processed data were not available at regular depths intervals or on a regular grid, in order to compare them with model solutions, the individual profiles were interpolated to a regular depth interval (0 to 2000 m), and compared with the closest point of the model grid. An hydrostatic correction was also implemented, i.e., pressure is converted to meters considering $\rho$=$\rho$(z). For the studied period (2003-2006), 2057 T/S profiles, from 49 buoys, were analyzed. The overall distribution of ARGO profiles and their Mean Absolute Error (MAE) is shown in figure 3, for the temperature (Fig. 3a) and salinity (Fig. 3b). Note that the MAE is depth averaged, between 0 to 2000 m. Location of ARGO profiles are represented by the colored data.

Sub-surface temperature and salinity data from three buoys from 'Puertos del Estado', Spain, were used for model validation. SST sensors were centered at 3 meters, and the buoys were located at the North-Eastern coast of Portugal (see localizations in the map of figure 8), where, Estaca de Bares is located at 7.58°W and 44.06°N; Villano Sisargas is located at 9.17°W and 43.50°N; and Cabo Silleiro is located at 9.44°W and 42.12°N.

### *2.3. Statistical metrics used for model validation*

At present, there are no standard protocols for the validation and evaluation of ocean model solutions. Therefore, as a first approach, and in order to compare model solutions with data, simple statistical metrics were used. Root Mean Squared Error (RMSE) is often used to quantify model accuracy for reproduction of ocean currents (Ivanov et al., 2009). The RMSE of the model solutions compared to observations can be expressed as (e.g. Pielke, 1984).

$$RMSE = \sqrt{\sum_{i=1}^{N} \frac{(\phi_m - \phi_o)^2}{N}} \quad (1)$$

Where, $\phi_m$ and $\phi_o$ are the values from model and observed, respectively; and $N$ is the number of analyzed values. Another statistical parameter that compares well the differences in averages between model values and observed values is the Mean Absolute Error (MAE; e.g. Stauffer and Seaman, 1990).

$$MAE = \sum_{i=1}^{N} \frac{|\phi_m - \phi_o|}{N} \quad (2)$$

On the other hand, the Bias, provides information about the model ability to overestimate or underestimate a variable, quantifying the model systematic error (e.g. Pielke, 1984)

$$Bias = \sum_{i=1}^{N} \frac{(\phi_m - \phi_o)}{N} \quad (3)$$

*2.4. Ocean Global Circulation Models (OGCM's) as boundary conditions*

One of the uses of OGCM's is to provide, boundary and initial conditions for high-resolution regional ocean models (Barth et al., 2008; Alvera-Azcárate et al., 2011). Currently, there are several OGCM solutions freely available for scientific and operational uses. In this study, four OGCM solutions were analyzed: (i) ECCO (Estimating the Circulation and Climate of the Ocean), with spatial resolution of one degree, and 10-days averaged solutions; (ii) SODA (Simple Oceanographic Data Assimilation), has a half-degree spatial

resolution and monthly averaged solutions; (iii) HYCOM (Hybrid Coordinate Ocean Model), with 1/12° spatial resolution, producing daily outputs; (iv) Mercator with a grid resolution of 1/4° and 3-days (mean) solutions. HYCOM and Mercator are considered to be eddy-resolving systems whereas SODA and ECCO are eddy-permitting but not eddy resolving, due to the limited spatial and temporal resolutions. The OGCM model details are summarized in table 2.

Mercator and HYCOM showed the lowest values of MAE and RMSE (see table 3, for comparative EKE values). The lowest bias is found for HYCOM and Mercator, and is negative for ECCO and SODA. Figure 2 shows that all OGCM's are able to reproduce the SST inter-annual variability (2004-2006), when comparing their solutions to both AVHRR and MW_SST. Also reproducible by all OGCMs is the fact that the summer of 2004 lasted longer than the subsequent summers. However, and as expected, the SST daily and weekly variability is only represented in HYCOM and Mercator solutions. Model data comparison is best with AVHRR than it is with MW_SST for most models except SODA, which compares best with MW_SST (RMSE is 0.33 for MW; 0.36 for AVHRR SST). Non-spite the fact that MW_SST is not limited by cloud coverage, AVHRR instruments have a stronger signal strength, furthermore AVHRR measures skin SST (10-20 $\mu m$) whereas MW sensors measures sub-skin SST ($\sim 1mm$)(e.g. Kawai and Wada, 2007), therefore MW sensors do not account for the surface skin effect. SST derived AVHRR is often cooler than the SST derived from the MW radiometer (e.g. Kawai and Wada, 2007). It is important to note that in the winter, in the northern midlatitudes, the AVHRR product is cooler than the in situ data,

and is warmer in summer (Reynolds et al., 2007), this cooling effect seems to be mimicked by most models.

From this analysis, both HYCOM and Mercator adequately represent the inter-annual, and in most cases the daily and/or weekly SST variability, in the NEA. Nevertheless, it often became very hard to access HYCOM database solutions, via the internet. Consequently, Mercator solution was selected as the most reliable global model solution, currently available to the authors, to be used for the mesoscale studies of historical events in the NEA.

## 3. Results and Discussions

### *3.1. Representing the right scales*

The Kolmogorov energy theory provides predictions on the shape of the energy spectrum of a 3D isotropic turbulent flow, this allows the quantification of energy present at a particular spatial scale (more details in Vallis, 2006). In the context of this study, this can help determine the scales being effectively resolved by the models. Vallis (2006) shows, for example, that energy will cascade to small scales following a $k^{-5/3}$ slope (Fig. 4, black line). Large scale flows are strongly anisotropic due to earth rotation and due to the vertical scales in the ocean being very small, compared to horizontal ones. In that regard, in the barotropic ocean the energy spectrum should follow the theory of geostrophic turbulence, thus enstrophy transfer should occur at $k^{-3}$ (Charney, 1971; Pedlosky, 1987; Vallis, 2006) (Fig. 4, black dashed-line).

As can be seen in figure 4, ROMS resolves more scales than the OGCM models. Therefore, in order to improve the OGCM solutions and study

(sub)mesoscale variability, there is a need to use high-resolution model grids. Comparing the OGCM solutions (figure 4), Mercator (1/4°) and HYCOM (not shown) resolve well up to the 100 km range, but it needs to be coupled with ROMS, in order to fully resolve the sub-mesoscale variability (10-100 km). On the other hand, ECCO and SODA are only representing larger scales (100-1000 km). Although this analysis is done for the same region, and for a particular (random) moment in time, it is not expected that it will vary much over space and time. Therefore, the ability of numerical ocean models to adequately resolve the energy spectrum for the different scales is very much a function its grid resolution. The enstrophy transfer which is diagnosed by $k^{-3}$, is only resolved by the higher resolution regional models i.e. ROMS.

There are also noticeable differences between the spectral density resolved by climatological forced regional model ($R\_C$) and the other ROMS solutions (e.g. $R\_M; R\_NQ$). Climatological forced ROMS resolve processes with lower spectral density signatures ($10^{-2} versus 10^{-1}$ revolved by the other ROMS experiments, $R\_M; R\_NQ$). Furthermore, the atmospherically forced ROMS show a greater turbulent variability, when compared with the climatologically forced experiment.

*3.2. Regional ocean circulation model validation*

The validation of our regional ocean circulation model was achieved studying some of the previously documented dynamics for the NEA critical subregions. First, the surface dynamics were studied by comparing model solutions with EKE, SST and buoys data. Secondly, the west propagation of

mesoscale eddies were studied comparing model to AVISO data. Thirdly, attention was given to the model reproducibility of the main NEA water masses. Finally, a case study of an Iberian Peninsula Upwelling episode, which occurred between the $5^{th}$ and the $20^{th}$ August of 2005, helped demonstrate the accuracy of the regional model solution to represent a specific oceanic event.

*3.2.1. Representation of surface dynamics*

Barth et al. (e.g. 2008), showed that OGCM boundary conditions improved the regional model solution, particularly on the shelf dynamics, even when the open boundary is located far, in the open ocean. Climatological forcing produced low-density gradients and less energetic regional solutions (Barth et al., 2008). Our results show that to adequately reproduce the interannual SST variability (see figures 5) another important factor to consider is the use of appropriate atmospheric forcing, such as better representative winds and heat fluxes. Likewise, in our study better SST comparisons were achieved using OGCM forced ROMS than climatological forced 17(Table 4). Experiments R_M and R_NQ show better comparisons with AVHRR derived SST data in relation to the purely climatologically forced experiment (R_C), (Fig. 5). The bias values are closer to 0 n R_M and R_NQ experiments, while the R_C experiment shows a greater variability. The RMSE values vary between 0 and 1 in R_M and R_NQ whereas in R_C it reaches 1.9. The analysis of the $r^2$ coefficient shows lowest correlation in winter months, probably due to limited data availability i.e. higher cloud coverage (e.g. Reynolds et al., 2007). Non-spite the fact that the satellite SST data uses OI to fill the missing values, it is expected the use of more SST valid data points during cloud

free periods, thus interpolated products are expected to have more accurate representation.

The comparisons between AVHRR derived SST and R_C worsens with time, 2003 RMSE and Bias are higher for 2006. Correlations are also weaker for 2006 than for the 2003-2005 period. Recent values of the DJFM NAO index, shows a progressive change for the same period (2003-2006). NAO indexes are -0.20 in the winter months of 2003, -0.11 in the winter of 2004, -0.82 in the winter of 2005, becoming 1.83 (positive) in the winter of 2006 (http://www.cru.uea.ac.uk/ timo/datapages/naoi.htm). In order to account for the inter-annual atmospheric variability, characteristic of periods with positive and negative NAO-years, it is important to consider non-climatological atmospheric forcing conditions. The leading mode of sea surface temperature (SST) variability over the North Atlantic during the positive NAO winter consists of a tripole pattern: (i) with a cold SST anomaly in the sub-polar region, (ii) a warm anomaly in the middle latitudes centered off Cape Hatteras (NEA case); (iii) a cold subtropical anomaly between the equator and $30 \circ N$ (Deser and Blackmon, 1993; Kushnir, 1994).

The temporal averaged SST shows the best model-data comparisons in the open-ocean (Fig. 6), thus there is a need to complement this analysis comparing model results with near-surface temperature collected using in situ buoys (see e.g. Barth et al., 2008; Ivanov et al., 2009). Variability of coastal (near-shore) processes are not well represented in merged/interpolated satellite products. The sub-surface (3m) temperature time-series of model solutions are in good agreement with the observations collected by the VS (Villano Sisargas), with the CS (Cabo Silleiro) and EB (Estaca de Bares)

buoys as shown in temporal series of temperature in figure 8. The ROMS experiments using high resolution atmospheric forcing (R_M and R_NQ) are able to reproduce the inter-annual variability in the buoys, whereas the climatologically forced experiment (R_C), showed always weaker correlations.

With respect to EKE derived from altimetry data, the best model representation is obtained in offshore regions and using climatological forcing conditions (figure 7). It is hypothesized that these differences are due to (i) the limited spatial and temporal resolution of AVISO data (1/3°), and (ii) due to the fact that the models have higher resolution compared to AVISO data, and thus they are more energetic. Furthermore, the lack of AVISO data near the coast favors the comparisons with offshore regions, since AVISO data accuracy is limited to acquire data up to 45 km from the coast (Durand et al., 2008).

*3.2.2. West propagation of eddies*

Figure 9, shows the westward propagation of mesoscale eddy structures (see white arrow in figure 9a and b), (34.0423 °N between 19 ° to 35 °W). Sangrà et al. (2009) observed two small corridors of westward propagating eddies, north and south of Azores Front. These corroborate the results showed in figures 9a and b. Also apparent, in our results, is the fact that these structures live less than 28 weeks ($\sim$ 200 days). Pingree and Sinha (2001), after analyzing infrared, altimeter and in-situ measurements, suggested that the westward movement of these large structures are due to cold (cyclonic) structures called STORMS, propagating westward around 32.2 °N. Thereafter, Pingree (2002) showed westward propagating anomalies (in their figure 3), occurring in the same area reproduced by our ROMS experiments

(figure 9c and d). Furthermore, there is good qualitative agreement between AVISO EKE data and the simulated EKE extracted from the R_M experiment. Moreover, the mesoscale structures observed in the figure 9c and d, correspond to the seasonal variability of EKE showed in Sangrà et al. (2009). The highest values of EKE are found south of the CA archipelago in spring, summer and autumn.

*3.2.3. Water masses reproducibility*

The waters masses described for the NEA are better depicted by the climatological forced regional model (R_C), and represented to a lesser degree of realism in the experiments using high resolution atmospheric forcing. It is expected that climatological forced ROMS best reproduces water masses composition due to its conservative nature. Deep-water masses with slow overturning rates, often takes hundreds of years for a complete re-circulation. On the other hand, this also challenges the classical view that atmospheric forcing only affects the ocean surface dynamics. Somehow, through vertical mixing (advection / diffusion), atmospheric forcing seems to also play an important role on water mass composition. In fact, there are recent examples in the literature suggesting that mesoscale surface-induced features, have a significant influence in 'venting' deep-water masses, perturbing its conservative flow regime.

The central water, North Atlantic Central Water (NACW; Fig. 10), characterized by density values of 27.38 ($kg/m^3$), with potential temperature varying ($\theta$) between 11-18 °C and salinities varying between 35.5-36.5 (Machín et al., 2006), showed good reproducibility by the model. However, the less reproducible water mass was indeed, the warmer and saltier Mediter-

ranean Intermediate Water (MIW; Fig.10). MIW is characterized by $\theta$ = 10 °C, with S higher than 35.6, and densities varying between 27.38-27.922 (kg/m$^3$) (Machín et al., 2006). The Antarctic Intermediate Water was also well represented in most regional models (AAIW; $\theta$ = [7-8] °C; S = [$<$ 35.4] and at $\gamma$ = [27.38-27.92] kg/m$^3$).

In terms of the different NEA sub-regions, the best correlation was found for the AF sub-region (Fig. 10a), with $r^2 \sim 0.99$, for temperature and $r^2 \sim 0.97$, for salinity. As expected the lowest correlation is found in MWO sub-region (Fig. 10b) where the $r^2$ are 0.94 and 0.86 for temperature and salinity, respectively. Despite the fact that CA and MA sub-regions are better correlated with ARGO profiles, than the IP sub-region, it is important to note that the CA and MA sub-regions had less profiles than the IP region and thus measured less intrinsic variability.

An overall statistical analysis was also performed for individual float trajectories in the whole NEA region. An example representative of these comparisons is shown in figures 11 a 16 , where the largest Bias between ROMS (R_C) solution and ARGO was often found in the sub-regions dominated by the MIW (between 1000 and 1700 m of depth) such as, AF (Fig. 11), MWO (Fig. 12) and IP (Fig. 13). However, better comparisons were found in regions away from the Gibraltar Strait namely: MA (Fig. 14), CA (Fig. 15) and AA (Fig. 16). Generally, in the three experiments simulations the values of Bias are in the range of -2 and 2 °C for temperature and -1 and 1 for salinity for each ARGO float comparison. These results, suggest that the poorest representation of the high salinity Intermediate Mediterranean Water in the model, i.e. the salinity was underestimated in ROMS.

The reason for these large differences are not in the number of sigma levels, since simulations with different numbers of sigma-levels were also considered, with no significantly different results. Nevertheless, there is a need to continue these experiments with coupled atmospheric-ocean models, considering a more realistic interchange between the atmosphere and the ocean. Haidvogel et al. (2000) suggests that without a continuous source of water with S>36.5, T>11.8 °C and °=27.9 kg/m$^3$, a significant freshening takes place during the model configuration, so the apparently better representation of MIW. Nevertheless, these corrections are often applied in longer model runs (+10 years), and thus apparently not so relevant for our 4 year NEA study. Peliz et al. (2007) and Mason et al. (2011), also prescribe the MIW outflow in the Gulf of Cadiz region, although this might be an acceptable band-aid parameterization, when using OGCM boundary conditions this might in fact compromise the initial and boundary conditions and thus introducing unexpected variability. To account for the inter-decadal variability of the MIW outflow, perhaps a better solution would be to reproduce such variability at the OGCM level, which would then propagate this onto the regional model solutions.

*3.2.4. Case study of an IPUS episode (Aug 2005)*

An Iberian upwelling event was detected with an 8-day MODIS-Aqua composite of surface derived chlorophyll-a (Fig. 17a), for the 20 of August 2005. The same episode was also captured in the AVHRR derived SST map, as shown in the figure 17b. For the same period, ROMS calculated SST (R_NQ) (Fig. 17c, d and e) showed similar low-temperatures suggesting the development of an upwelling event, accompanied by the formation of an

upwelling filament, in the Extremadura promontory (between 38.5 and 39.5 °N, 17c). The same event was previously studied by Meunier et al. (2010) using SST and chlorophyll maps. Peliz et al. (2003) observed that in such events eddy shedding might occur as a result of the interaction between the flow with the topography discontinuities, like the Extremadura promontory, coherent with the location of some SST fronts. Recently, Batteen et al. (2007) identified three main reasons to explain the generation of filaments which include: (i) the baroclinic instability of the upwelling front; (ii) the effect of capes and promontories; (iii) planetary beta effect and bottom topography.

In fact, all our ROMS simulations can reproduce lowest temperatures near the coast, suggesting the development of an IPUS event, however, R_M and R_NQ (Fig. 17c and d), computed the best results. The black box in the top panel of figure 8 highlights the strong upwelling event (see clorophyll-a map in figure 17a) for the VS buoy. The second black box represents the data collected by the CS buoy, also denoting another IPUS event (August, 2006). These results show that the experiments including adequate atmospheric forcing, are capable of reproducing the inter-annual variability measured by the buoys. The same can not be said for the climatological experiment R_C which maintains a constant temperature, during both IPUS events. Quantitatively, the lowest spatial RMSE was found using R_M, with an average value of 0.73 °C for the whole month of August, instead of 1.06 °C and 1.27 °C for R_NQ and R_C, respectively. As is expected, Bias values are also lower for the R_M (0.42 °C) and for the R_NQ (0.65 °C), compared to the R_C experiment (0.91 °C).

## 4. Conclusions and suggestions for future works

1 - The results from this work show the importance of atmospheric fluxes to generate a realistic regional ocean model solution for the NEA. There are also some advantages on downscaling an OGCM solution into a regional model to study the dynamics of the mesoscale processes and not relying only on climatological forcing. Current OGCM solutions of eddy-resolving ($1/12^{\circ}$), are only available from 2009 to the present. The kinetic energy spectra (Fig. 4) shows that ROMS seems to reconstitute the theoretical spectrum of oceanic mesoscale, representing the slopes $k^{-5/3}$ and $k^{-3}$, according to Kolmogorov turbulent cascade energy. The effective resolution of OGCM is at scales of $\sim 500km$ for SODA, $\sim 600km$ for ECCO and $\sim 100km$ for Mercator, where the energy levels drops down the slope of $k^{-3}$.

2 - The statistical analysis show a good data-model comparisons, with SST and EKE derived from satellite data, except in coastal areas where the satellite detection capability is limited. The better correlations are found in offshore regions. Is equally important to note that model-data comparisons with AVHRR derived SST, showed better statistical agreement, than when comparing model with $MW\_SST$ data. Model comparisons with in-situ buoy data, R_M and R_NQ reproduced well the daily sub-surface variability (Fig. 8).

3 - ROMS numerical experiments also replicate, rather well, the detection the eddy corridors documented in Sangrà et al. (2009), using altimetry data extracted from AVISO. This eddies propagate westward as originally proposed by Pingree (2002) and recently confirmed by Sangrà et al. (2009).

4 - The water column composition is best represented using ROMS forced

with climatological data. The central and deep waters, represented by R_C are in good agreement with the ARGO profiles, whereas the depth of occurrence of the Mediterranean Intermediate Water (MIW) is not as accurately represented, since ROMS underestimates the highest salinity values.

5 - The analysis of the results also show that ROMS forced with high temporal resolution atmospheric fluxes (experiments R_NQ and R_M), reproduces well an IPUS event, (20 of August of 2005). Realistic upwelling filaments are also well simulated, representing the interaction of the flow and the local topography, along the Iberian Peninsula coast.

Future works include, but are not limited to, the use of coupled a ocean-atmospheric mode, in order to study the surface dynamics without compromising the water masses representativity. It is also expected that the inclusion of tides and river outflows, will contribute for a better representation of the salinity values, in particular the adequate location of MIW.

## 5. Acknowledgments

The authors wish to acknowledge funds from projects: RAIA ($0313\_RAIA\_1\_E$) and PROMECA (CTM2009-06993-E/MAR). Numerical model solutions were calculated at CIIMAR HPC unit, constructed using funds the FCT-Portuguese National Science Foundation pluriannual, and further improved using funds from RAIA.co project, co-funded by INTERREG-IV and by FEDER ('Fundo Europeu de Desenvolvimento Regional, 2007-2013'), through the POCTEP regional initiative. The altimeter products were produced by SSALTO/DUACS and distributed by AVISO with support from CNES. MODIS data was extracted using the online system, developed and maintained by the NASA.

## References


Alvarez, I., Ospina-Alvarez, N., Pazos, Y., deCastro, M., Bernardez, P., a. C. M. J., Gomez-Gesteira, J. L., Alvarez-Ossorio, M. T., Varela, M., Gomez-Gesteira, M., Prego, R., 2009. A winter upwelling event in the northern galician rias: Frequency and oceanographic implications. Estuarine, Coastal and Shelf Science 82 (4), 573–582.

Alvera-Azcárate, A., Barth, A., Weisberg, R. H., Castaeda, J. J., Vandenbulcke, L., Beckers, J. M., 2011. Thermocline characterisation in the cariaco basin: A modelling study of the thermocline annual variation and its relation with winds and chlorophyll-a concentration. Continental Shelf Research 31, 73–84.

Alves, M. L. G. R., De Verdière, A. C., 1999. Instability dynamics of a subtropical jet and applications to the azores front current system: Eddy-driven mean flow. Journal of Physical Oceanography 29 (5), 837–864.

Antonov, J. I., Locarnini, R. A., Boyer, T. P., Mishonov, A. V., Garcia, H. E., 2006. World ocean atlas 2005, volume 2: Salinity. s. levitus. Tech. rep., Ed. NOAA Atlas NESDIS 62, U.S. Government Printing Office, Washington, D.C., 182 pp.

Armi, L., Stommel, H., 1983. Four views of a portion of the north atlantic subtropical gyre. Journal of Physical Oceanography 13 (5), 828–857.

Bahurel, P., Dombrowsky, E., Lellouche, J. M., project team, M. (Eds.), 2004. Mercator ocean monitoring and forecasting system, near-realtime assimi-

lation of satellite and in-situu data in different operational ocean models. Proc. 36th International Colloquium on Ocean dynamics, Lige, Belgium.

Barth, A., Alvera-Azcárate, A., Weisberg, R. H., 2008. Benefit of nesting a regional model into a large-scale ocean model instead of climatology. application to the west florida shelf. Continental Shelf Research 28 (4-5), 561–573.

Barton, E. D., Inall, M. E., Sherwin, T. J., Torres, R., 2001. Vertical structure, turbulent mixing and fluxes during lagrangian observations of an upwelling filament system off northwest iberia. Progress in Oceanography 51 (2-4), 249–267.

Batteen, M. L., Martinho, A. S., Miller, H. A., McClean, J. L., 2007. A process-oriented modelling study of the coastal canary and iberian current system. Ocean Modelling 18 (1), 1–36.

Beckmann, A., Haidvogel, D. B., 1993. Numerical simulation of flow around a tall isolated seamount. part i: problem formulation and model accuracy. Journal of Physical Oceanography 23 (8), 1736–1753.

Charney, J. G., 1971. Geostrophic turbulence. Journal of Atmosphere Society 28, 1087–1095.

Chelton, D. B., Schlax, M. G., Samelson, R. M., de Szoeke, R. A., 2007. Global observations of large oceanic eddies. Geophysical Research Letters 34 (15).

da Silva, A. M., Young, C. C., Levitus, S., 1994. Atlas of surface marine data

1994. Tech. rep., Tech. Rep. NOAA/NESDIS Atlases 6-10, U.S. Department of Commerce, NOAA, NESDIS.

Deser, C., Blackmon, M. L., 1993. Surface climate variations over the north atlantic ocean during winter: 1900-1989. Journal of Climate 6 (9), 1743–1753.

Durand, F., Shankar, D., Birol, F., Shenoi, S., 2008. Estimating boundary currents from satellite altimetry: A case study for the east coast of india. Journal of Oceanography 64 (6), 831–845.

Fairall, C. W., Bradley, E. F., Hare, J. E., Grachev, A. A., Edson, J. B., 2003. Bulk parameterization of air-sea fluxes: Updates and verification for the coare algorithm. Journal of Climate 16 (4), 571–591.

Fairall, C. W., Bradley, E. F., Rogers, D. P., Edson, J. B., Young, G., 1996. Bulk parameterization of air-sea fluxes for tropical ocean global atmosphere coupled-ocean atmosphere response experiment. J. Geophys. Res. C: Oceans 101 (C2), 3747–3764.

Haidvogel, D. B., Arango, H. G., Hedstrom, K., Beckmann, A., Malanotte-Rizzoli, P., Shchepetkin, A. F., 2000. Model evaluation experiments in the north atlantic basin: Simulations in nonlinear terrain-following coordinates. Dynamics of Atmospheres and Oceans 32 (3-4), 239–281.

Haidvogel, D. B., Beckmann, A., HedStrm, K. S., 1991. Dynamical simulations of filament formation and evolution in the coastal transition zone. Journal Geophysical Research 96, 15017–15040.

Haynes, R., Barton, E. D., Pilling, I., 1993. Development, persistence, and variability of upwelling filaments off the atlantic coast of the iberian peninsula. Journal of Geophysical Research 98 (C12), 22,681–22,692.

Ivanov, L. M., Collins, C. A., Marchesiello, P., Margolina, T. M., 2009. On model validation for meso/submesoscale currents: Metrics and application to roms off central california. Ocean Modelling 28 (4), 209–225.

Jochum, M., Danabasoglu, G., Holland, M., Kwon, Y. O., Large, W. G., 2008. Ocean viscosity and climate. Journal of Geophysical Research C: Oceans 113 (6).

Kawai, Y., Wada, A., 2007. Diurnal sea surface temperature validation and its impact on the atmosphere and ocean: A review. Journal Oceanography 63, 721–744.

Klein, B., Siedler, G., 1989. On the origin of the azores current. Journal Geophysical Research 94, 6159–6168.

Kushnir, Y., 1994. Interdecadal variations in north atlantic sea surface temperature and associated atmospheric conditions. Journal of Climate 7 (1), 141–157.

Large, W. G., McWilliams, J. C., Doney, S. C., 1994. Oceanic vertical mixing: A review and a model with a nonlocal boundary layer parameterization. Reviews of Geophysics 32 (4), 363–403.

Le Traon, P. Y., De Mey, P., 1994. The eddy field associated with the azores front east of the mid- atlantic ridge as observed by thegeosat altimeter. j. geophys. res. 99, 99079923. Journal Geophysical Research.

Locarnini, R. A., Mishonov, A. V., Antonov, J. I., Boyer, T. P., Garcia, H. E., 2006. World ocean atlas 2005, volume 1: Temperature. s. levitus. Tech. rep., Ed. NOAA Atlas NESDIS 61, U.S. Government Printing Office, Washington, D.C., 182 pp.

Machín, F., Hernández-Guerra, A., Pelegrí, J. L., 2006. Mass fluxes in the canary basin. Progress in Oceanography 70 (2-4), 416–447.

Marchesiello, P., Debreu, L., Couvelard, X., 2009. Spurious diapycnal mixing in terrain-following coordinate models: The problem and a solution. Ocean Modelling 26 (3-4), 156–169.

Marchesiello, P., McWilliams, J. C., Shchepetkin, A., 2001. Open boundary conditions for long-term integration of regional oceanic models. Ocean Modelling 3 (1-2), 1–20.

Mason, E., Colas, F., Molemaker, J., Shchepetkin, A. F., Troupin, C., McWilliams, J. C., Sangrà, P., 2011. Seasonal variability of the canary current: A numerical study. Journal of Geophysical Research C: Oceans 116 (6).

Mauritzen, C., Morel, Y., Paillet, J., 2001. On the influence of mediterranean water on the central waters of the north atlantic ocean. Deep-Sea Research Part I: Oceanographic Research Papers 48 (2), 347–381.

Melsom, A., Lien, V. S., Budgell, W. P., 2009. Using the regional ocean modeling system (roms) to improve the ocean circulation from a gcm 20th century simulation. Ocean Dynamics 59 (6), 969–981.

Meunier, T., Rossi, V., Morel, Y., Carton, X., 2010. Influence of bottom topography on an upwelling current: Generation of long trapped filaments. Ocean Modelling 35 (4), 277–303.

Pedlosky, J., 1987. Geophysical Fluid Dynamics, 2nd Edition. Springer-Verlag, New York.

Peliz, A., Dubert, J., Haidvogel, D. B., Le Cann, B., 2003. Generation and unstable evolution of a density-driven eastern poleward current: The iberian poleward current. Journal of Geophysical Research C: Oceans 108 (8), 24–1.

Peliz, A., Dubert, J., Marchesiello, P., Teles-Machado, A., 2007. Surface circulation in the gulf of cadiz: Model and mean flow structure. Journal of Geophysical Research C: Oceans 112 (11).

Peliz, A., Rosa, T. L., Santos, A., Miguel, P., Pissarra, J. L., 2002. Fronts, jets, and counter-flows in the western iberian upwelling system. Journal of Marine Systems 35 (1-2), 61–77.

Penven, P., 2003. ROMSTOOLS users guide. Technical report. Institut de Recherche pour le De`veloppement, 213 rue Lafayette, Paris, France.

Pielke, R. A., 1984. Mesoscale Meteorological Modeling, 1st Edition. Academic Press, New York.

Pingree, R., 2002. Ocean structure and climate (eastern north atlantic): In situ measurement and remote sensing (altimeter). Journal of the Marine Biological Association of the United Kingdom 82 (5), 681–707.

Pingree, R., Sinha, B., 2001. Westward moving waves or eddies (storms) on the subtropical/azores front near 32.5n? interpretation of the eulerian currents and temperature records at moorings 155 (35.5w) and 156 (34.4w). Journal of Marine Systems 29 (1-4), 239–276.

Pollard, R., Griffiths, M. J., Cunningham, S. A., Read, J. F., Prez, F. F., Ros, A. F., 1996. Vivaldi 1991 - a study of the formation, circulation and ventilation of eastern north atlantic central water. Progress in Oceanography 37 (2), 167–192.

Relvas, P., Barton, E. D., Dubert, J., Oliveira, P. B., Peliz, A., da Silva, J. C. B., Santos, A. M. P., 2007. Physical oceanography of the western iberia ecosystem: Latest views and challenges. Progress in Oceanography 74 (2-3), 149–173.

Reynolds, R. W., Smith, T. M., 1994. Improved global sea surface temperature analyses using optimum interpolation. Journal of Climate 7 (6), 929–948.

Reynolds, R. W., Smith, T. M., Liu, C., Chelton, D. B., Casey, K. S., Schlax, M. G., 2007. Daily high-resolution-blended analyses for sea surface temperature. Journal of Climate 20 (22), 5473–5496.

Sangrà, P., Pascual, A., Rodríguez-Santana, A., Machín, F., Mason, E., McWilliams, J. C., Pelegrí, J. L., Dong, C., Rubio, A., Arístegui, J., Marrero-Díaz, A., Hernández-Guerra, A., Martínez-Marrero, A., Auladell, M., 2009. The canary eddy corridor: A major pathway for long-lived eddies

in the subtropical north atlantic. Deep-Sea Research Part I: Oceanographic
695 Research Papers 56 (12), 2100–2114.

Shchepetkin, A. F., Mcwilliams, J. C., 1998. Quasi-monotone advection schemes based on explicit locally adaptive dissipation. Monthly Weather Review 126 (6), 1541–1580.

Shchepetkin, A. F., McWilliams, J. C., 2003. A method for computing hori-
700 zontal pressure-gradient force in an oceanic model with a nonaligned vertical coordinate. Journal of Geophysical Research C: Oceans 108 (3), 35–1.

Shchepetkin, A. F., McWilliams, J. C., 2005. The regional oceanic modeling system (roms): A split-explicit, free-surface, topography-following-coordinate oceanic model. Ocean Modelling 9 (4), 347–404.

705 Song, Y., Haidvogel, D., 1994. Numerical simulations of the ccs under the joint effects of coastal geometry and surface forcing. pp. 216–234.

Stauffer, D. R., Seaman, N. L., 1990. Use of four-dimensional data assimilation in a limited-area mesoscale model. part i: experiments with synoptic-scale data. Monthly Weather Review 118 (6), 1250–1277.

710 Vallis, G. K., 2006. Atmospheric and Oceanic Fluid Dynamics. Cambridge University Press.

Volkov, D. L., Fu, L. L., 2010. On the reasons for the formation and varibiality of the azores current. Journal Geophysical Oceanography 40, 2197–2220.

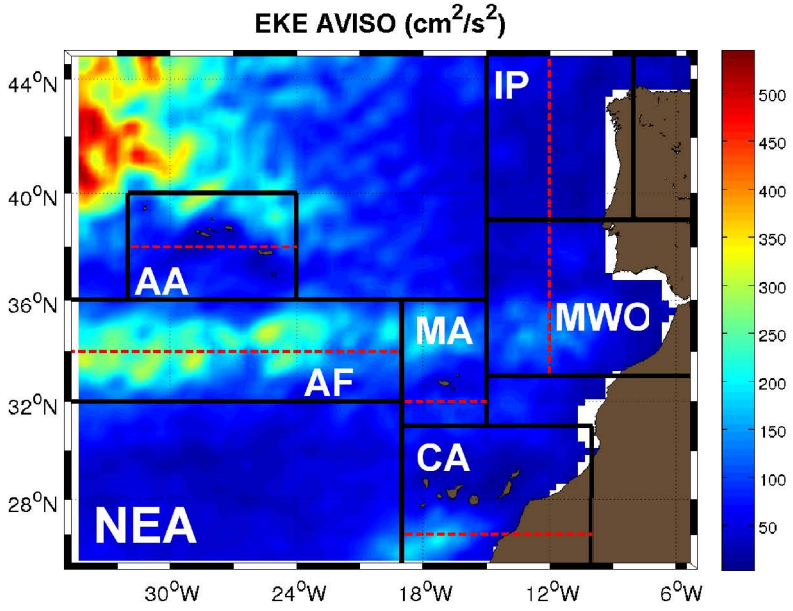


Figure 1: Eddy Kinetic Energy (EKE) computed from AVISO data (average 2003-2006 years) for NEA domain. The black boxes denote the critical sub-regions used for the solution validation, where: AF-Azores Front; MWO-Mediterranean Water Outflow; IP-Iberian Peninsula; MA- Madeira Archipelago; CA-Canary Archipelago; and AA-Azores Archipelago. Dashed red lines show the sections used to plot of the Hövmoeller diagrams.

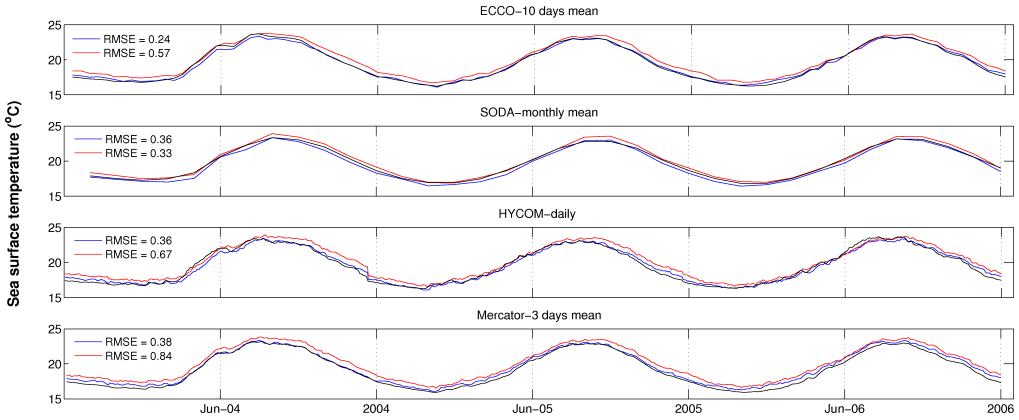


Figure 2: Temporal series of Sea Surface Temperature (°C) for each OGCM (black line) compared with SST from AVHRR (blue line) and MW_SST (red line) for the period of time since 2004 to 2006 where (a) is ECCO model; (b) SODA model; (c) HYCOM model and (d) Mercator model. One can note the differences in their temporal resolutions.

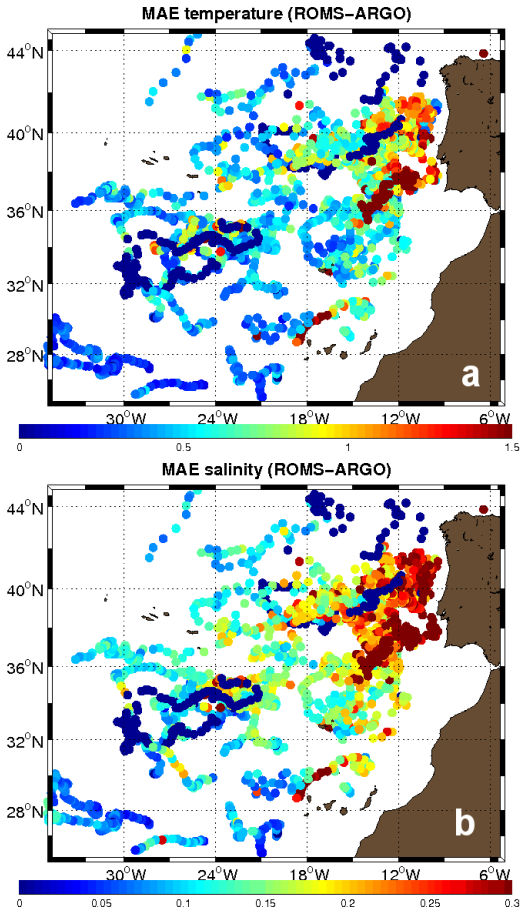


Figure 3: (a) Depth average MAE of temperature profiles between ARGO and ROMS profiles (0 to 2000 m averaged) for the 2003 to 2006 period of study. (b) MAE for salinity profiles.

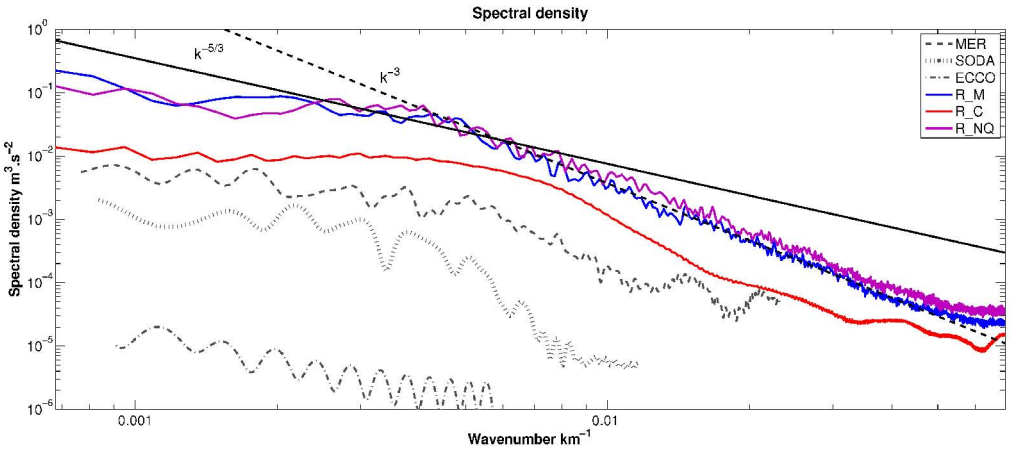


Figure 4: Kinetic energy spectra ($m^3/s^{-2}$) of three OGCM models: Mercator (1/4 degree; gray dashed line); SODA (1/2 degree; gray dot line); ECCO (1 degree; gray dashed-dotted line); and the three ROMS simulation experiments: R_M run (1/12 degree; blue line); R_NQ (1/12 degree; violet line); and R_C run (1/12 degree; red line) for all domain at 35° N Latitude and for one month of simulation in Jan-2003. The spectra show how ROMS seems to reconstitute the theoretical spectrum of oceanic mesoscale represented by the slopes -5/3 (solid black line) and -3 (dashed black line).

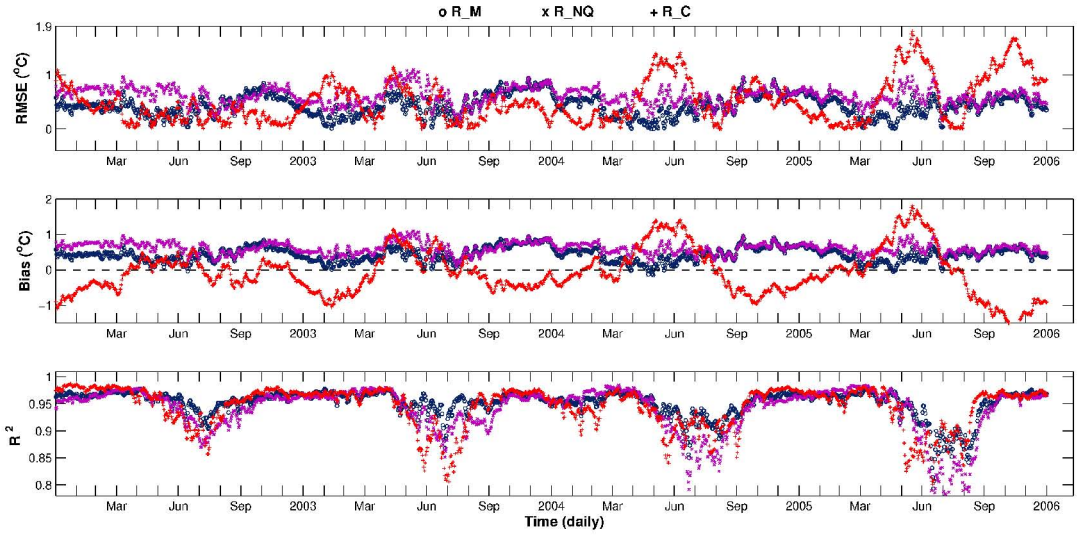


Figure 5: Temporal series of Root Mean Squared Error (top panel), Bias (middle panel) and correlation coefficients (bottom panel) for the whole area of NEA and during the four simulated years (2003-2006), between the three experiments made for this study and SST from AVHRR, where blue (o) are R_M, violet (x) are R_NQ and red (+) are R_C.

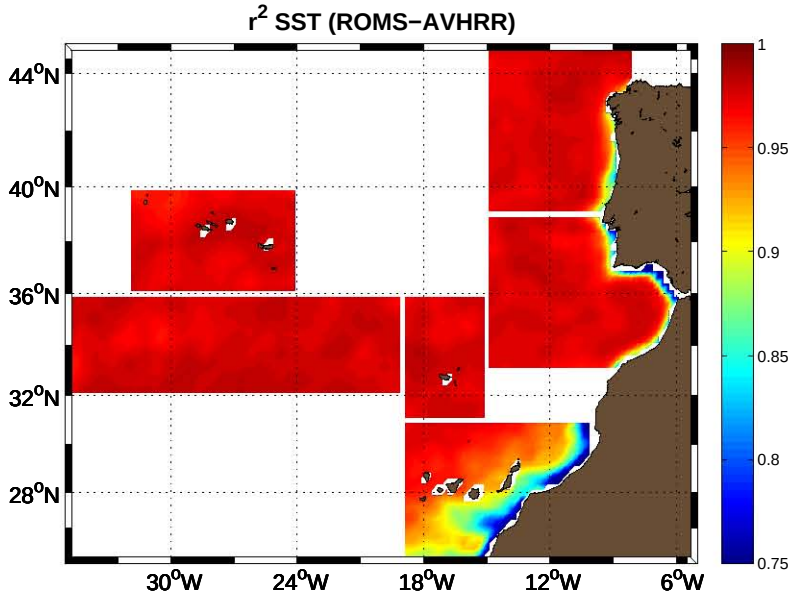


Figure 6: (a). Temporal averages of correlation coefficient ($r^2$), for four years since 2003, comparing SST from R_M experiment results with SST from AVHRR satellite data, computing for each sub-region.

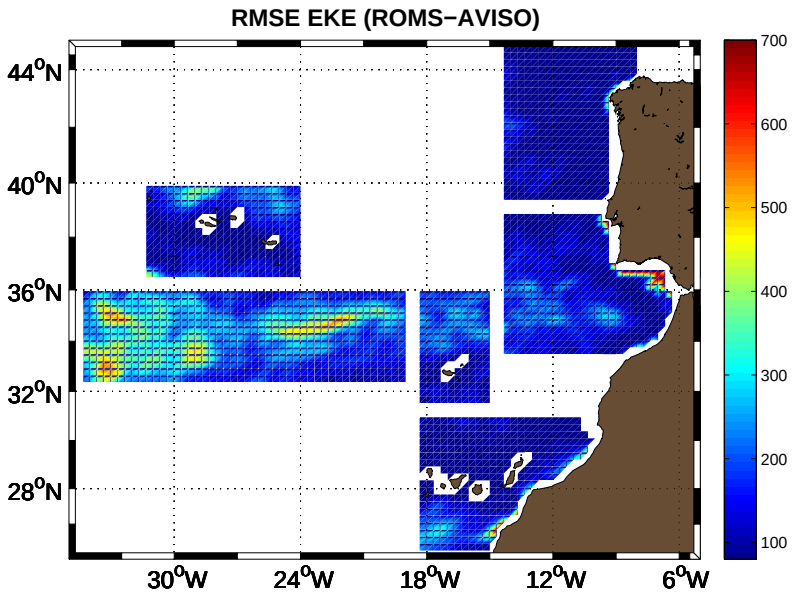


Figure 7: Temporal averages of Root Mean Squared Error (RMSE) for four years since 2003, between EKE from R_M experiment and AVISO altimeter data, computed to each sub-region. Units are in $cm^2/s^2$

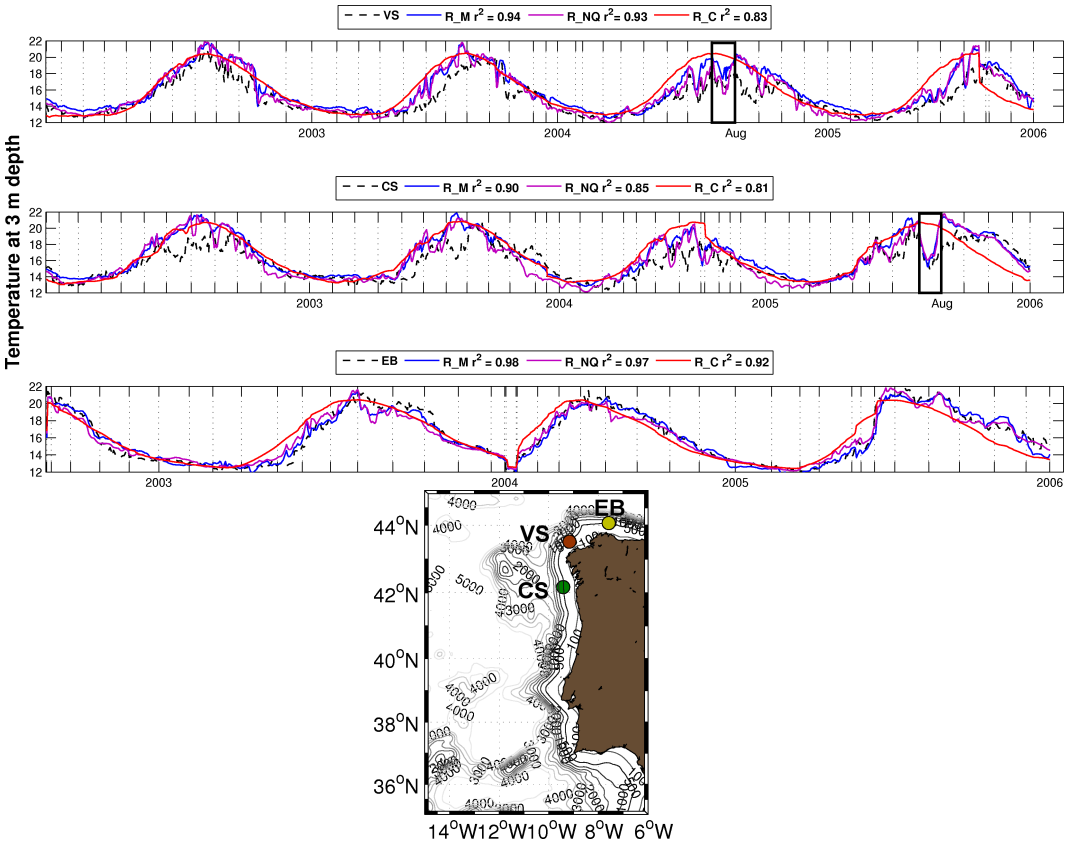


Figure 8: Temporal series during 2003-2006 of temperature at 3 m depth from Puertos del Estado buoys (black dashed lines): Villano Sisargas (VS), Cabo Silleiro (CS) and Estaca de Bares (EB) compared at the same depth with R_M (blue line), R_NQ (violet line) and R_C (red line). Mean values of correlation coefficients are also showed in the top of these figures, higher values were archived for R_M and R_NQ than for the R_C run. Black boxes correspond to an IPUS event of August 2005 for VS buoy and other at August 2006 for CS buoy. Note that the temporal axis are not always the same due the miss data in some days of the buoy. The location of the three Puertos del Estado buoys are also shown in the bottom panel with the bathymetry of the area.

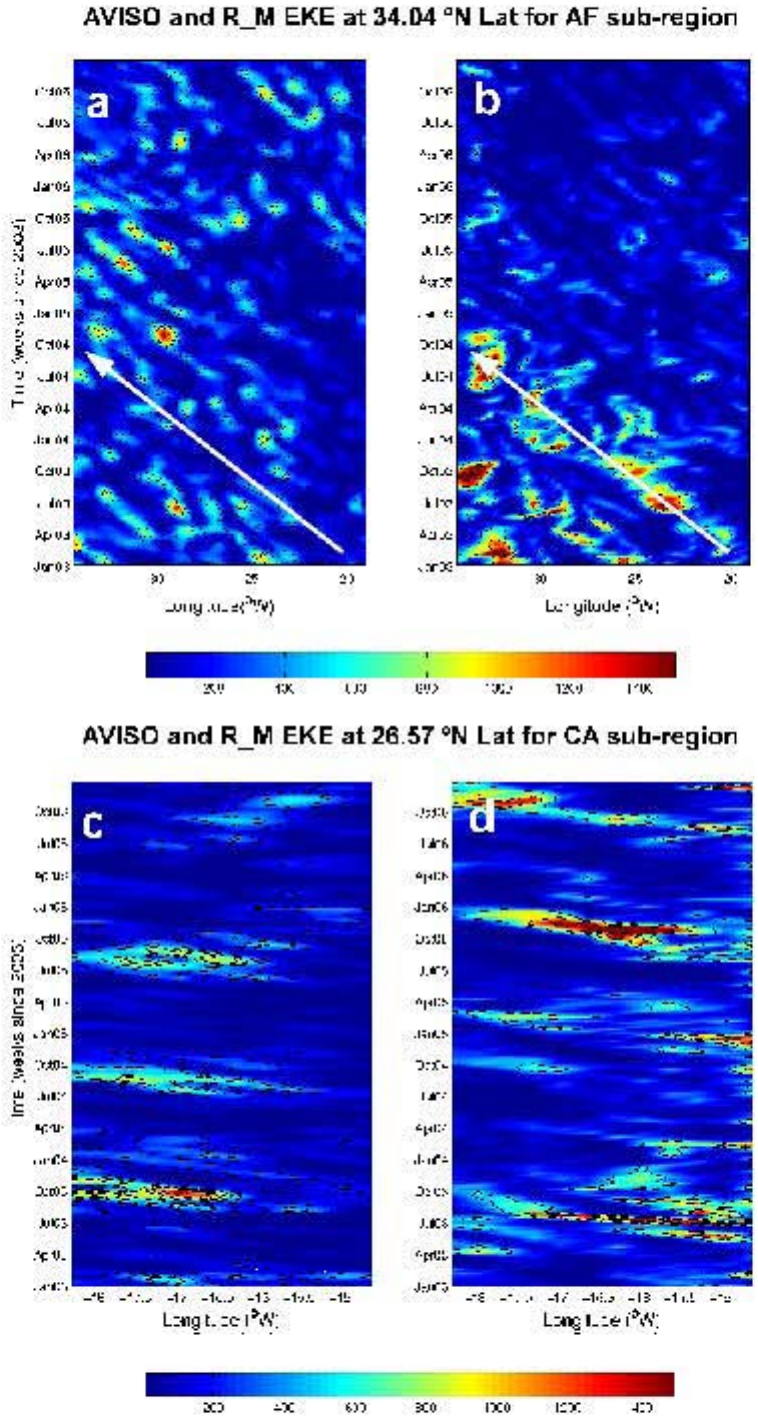


Figure 9: Longitude/time Hövmoeller plot showing four years (2003-2006) of monthly means EKE between AVISO data and the experiment R_M, where (a) AVISO data for AF sub-region compared to (b) R_M for AF sub-region; (c) AVISO EKE data for CA sub-region compared to (d) R_M EKE for CA sub-region White arrows shown the westward direction of mesoscale structures. Latitudes selected to make these figures can be seen in the red lines of figure 1.

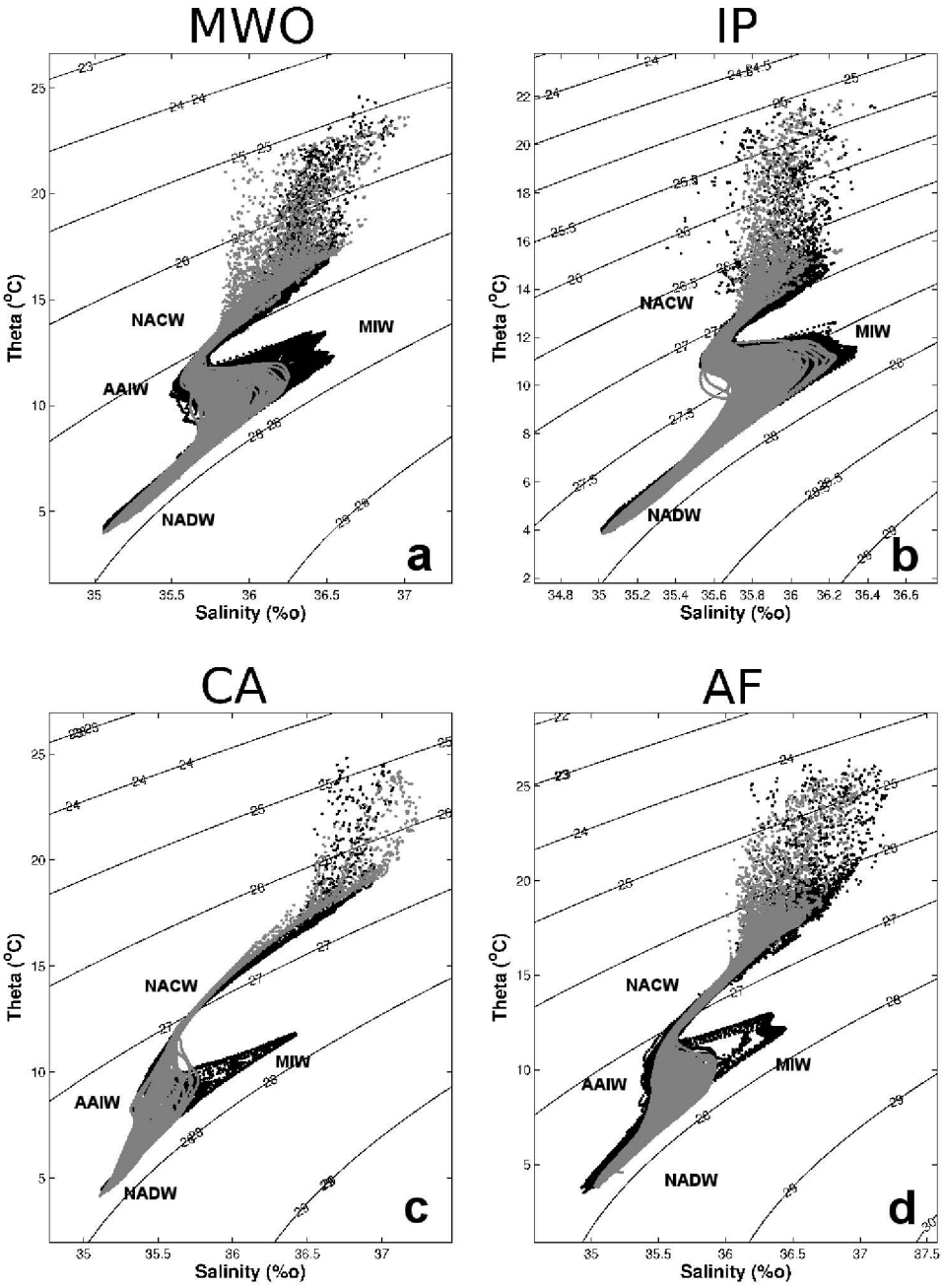


Figure 10: Theta-S diagrams from 0 to 2000 m depth for all ARGO profiles (black diagrams) available for a period from 2003 to 2006 in some sub-regions compared with R_C profiles (gray diagrams) at the same or very near location of each ARGO profiles, where (a) represented the MWO sub-region with 9 floats and 345 profiles, (b) IP sub-region represented with 8 floats and 331 profiles, (c) CA sub-region represented with 2 floats and 57 profiles, and (d) AF sub-region represented with 8 floats and 446 profiles. Mainly water masses present in the NEA region are written in each diagram.

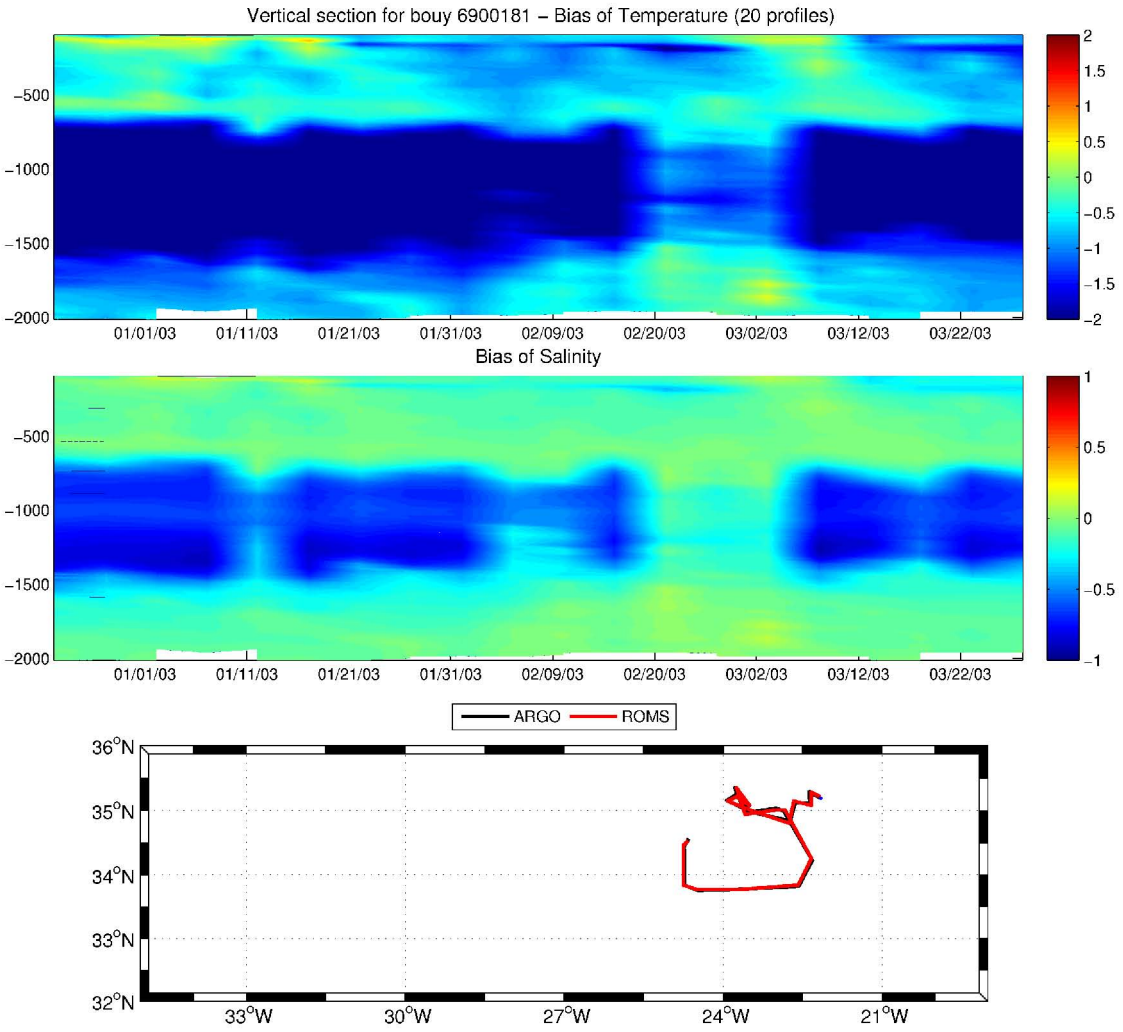


Figure 11: Vertical section of Bias between profiles from R_C simulation and profiles from ARGO buoy (number 6900181) in the AF sub-region, for temperature (top) and salinity (middle). The trajectory for both ROMS (black) and ARGO (red) are in the map (bottom), where the blue point denoted the first profile of this buoy.

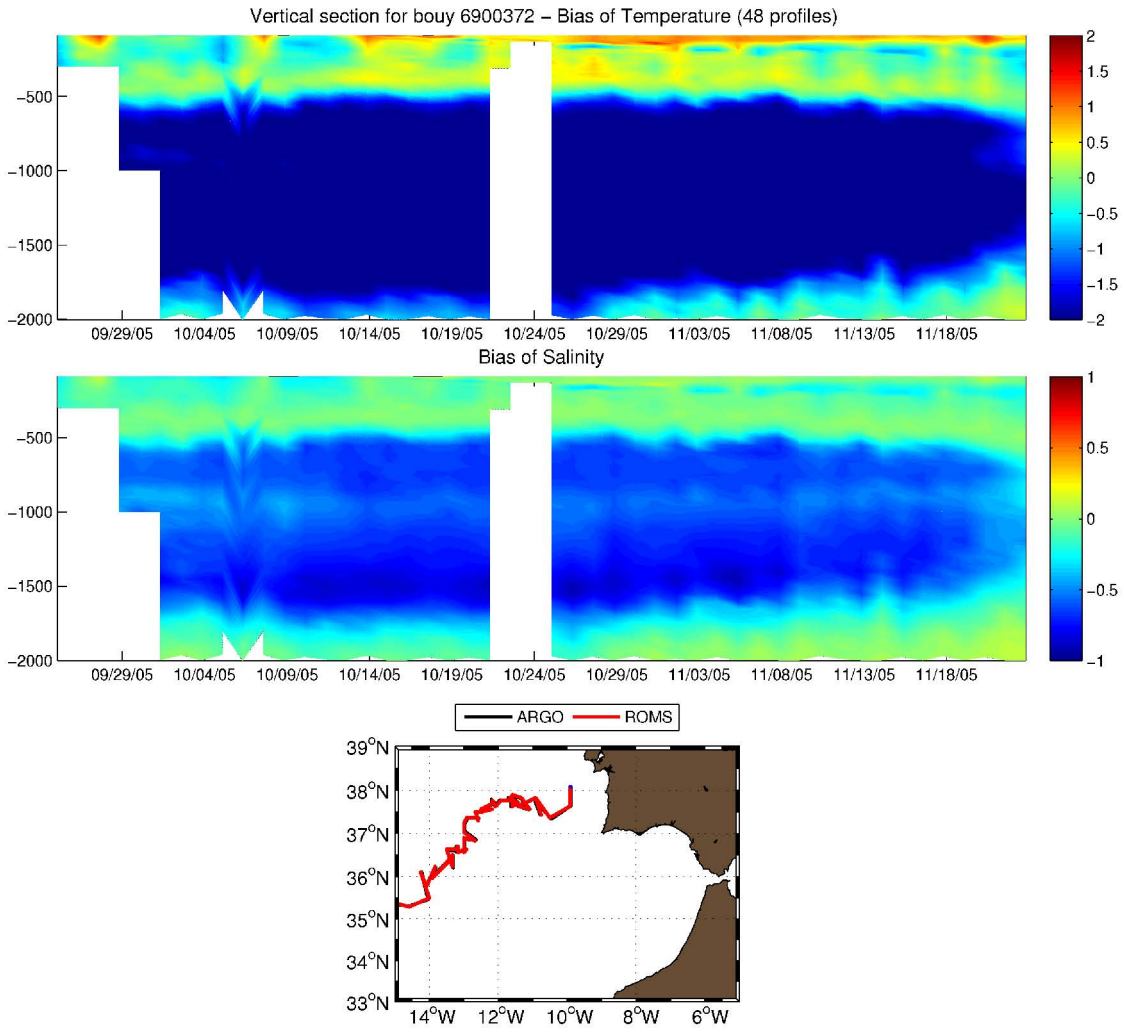


Figure 12: ARGO buoy number 6900372 in the MWO sub-region.

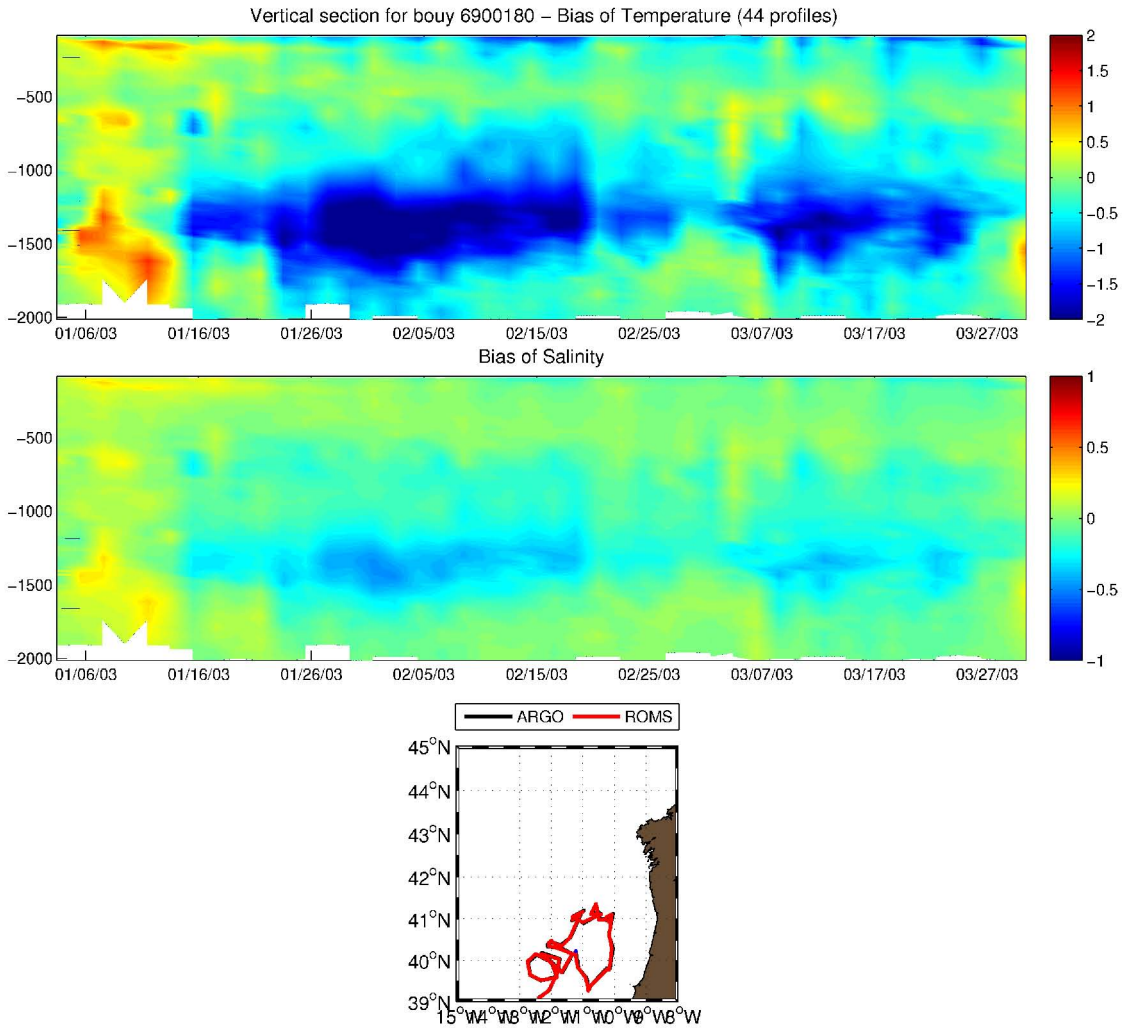


Figure 13: ARGO buoy number 6900180 in the IP sub-region.

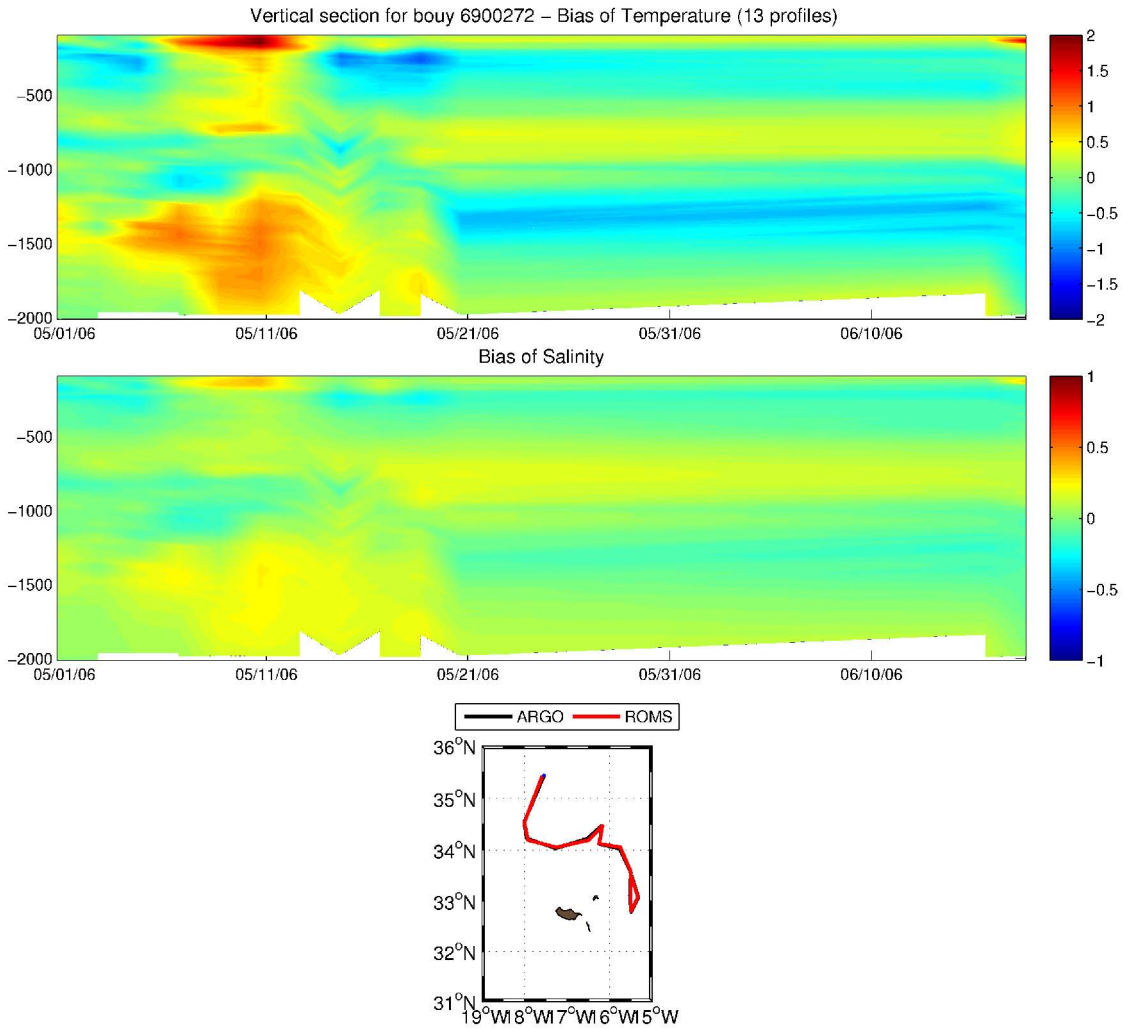


Figure 14: ARGO buoy number 6900272 in the MA sub-region.

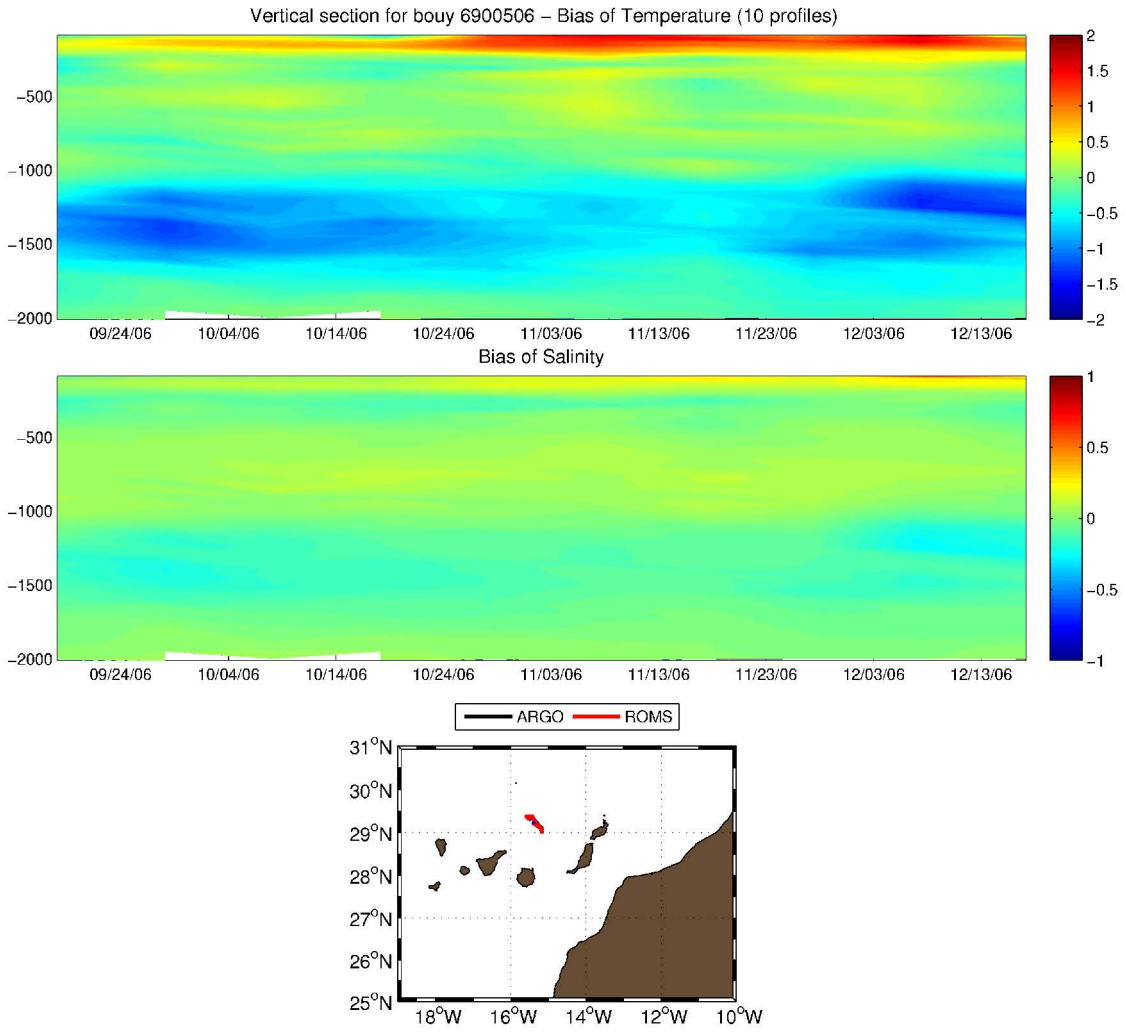


Figure 15: ARGO buoy number 6900506 in the CA sub-region.

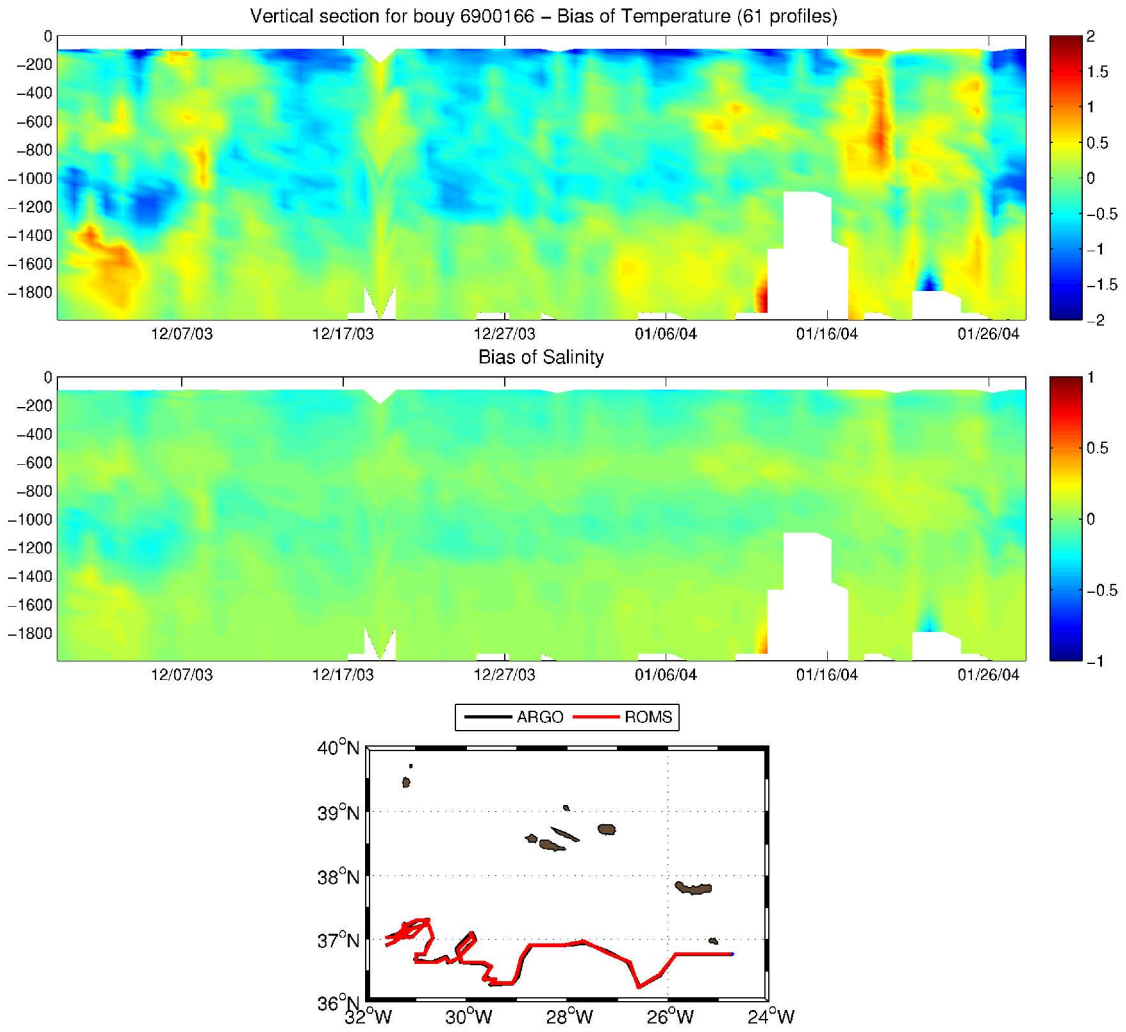


Figure 16: ARGO buoy number 6900166 in the AA sub-region.

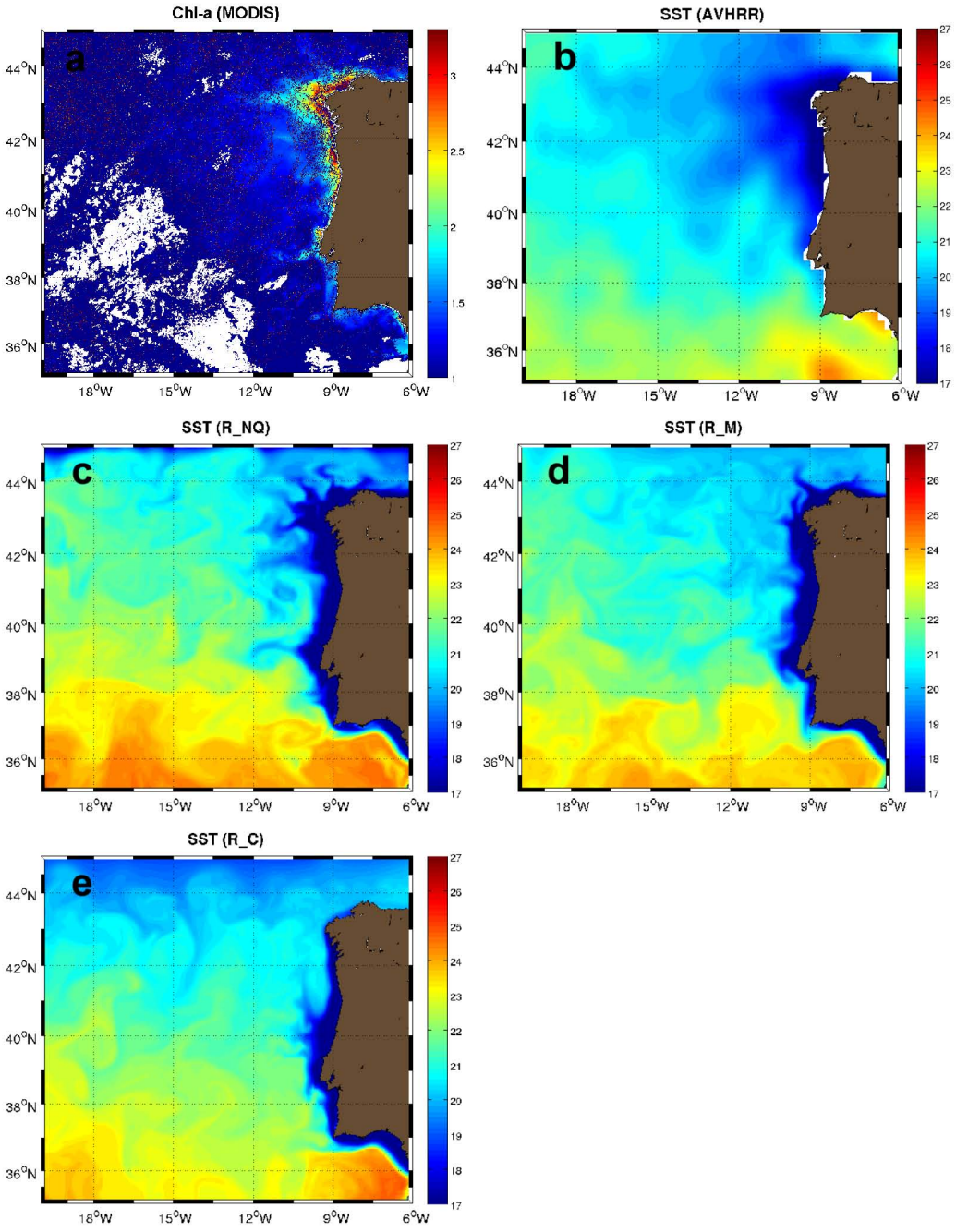


Figure 17: (a) Map of chlorophyll-a concentration (log10*100 mg/m$^3$) from MODIS for 8 days averages (13 to 20 August 2005) indicating an IPUS event in the Iberian Peninsula coast. (b) SST °C from AVHRR at 20 Aug 2005 show the same upwelling event. (c), (d) and (e) maps of SST °C from the experiment R_NQ, R_M and R_C, respectively, for the same IPUS event of 20 Aug 2005.

Table 1: Sources of data used in this study for the validations and comparison with the different ocean models

| **Data** | **Source** | **Available period of time** | **Spatial resolution** | **Temporal resolution** |
|---|---|---|---|---|
| EKE from SLA | AVISO | 2003-2006 | 1/3º x 1/3º | Weekly |
| SST | AVHRR | Jan-1985 to present | 1/4º x 1/4º | Daily |
| | MW_SST | Jun-2002 to present | 1/4º x 1/4º | Daily |
| Temperature and salinity profiles | ARGO floats | 2003-2006 | Irregular grid<br>2057 profiles from 49 floats | |
| Temporal serie of temperature | Puertos del Estado buoys | 2003-2006 | 3 buoys in the North-East part of Iberian Peninsula at 3 m of depth | |

Table 2: Mainly characteristic of different OGCMs used in this study

| **Characteristic of OGCMs** | **ECCO** | **SODA** | **HYCOM** | **Mercator** |
|---|---|---|---|---|
| Data assimilation | Yes | Yes | No | No |
| Experiment | ECCO-JPL | V2.0.4 | Exp. 05.8 | PSY2V3R1 |
| Spatial resolution | 1º x 1º | 1/2º x 1/2º | 1/12º x 1/12º | 1/4º x 1/4º |
| Temporal resolution | Mean 10 days | Monthly mean | Daily | Mean 3 days |
| Available period | 1993-on going | 1958-2007 | 2003-2006 | 2003-2006 |
| References | Stammer and Chassignet, 2000 | Carton and Giese, 2008 | Chassignet et al., 2007 | Bahurel et al., 2004 |
| Source download | http://ecco.jpl.nasa.gov | http://iridl.ldeo.columbia.edu/SOURCES/.CARTON-GIESE/.SODA/.v2p0p2-4 | http://tds.hycom.org | under contract delivery from Mercator-OCEAN www.mercator-ocean.fr |

Table 3: Temporal means of statistic parameters: MAE (Mean Absolute Error); RMSE (Root Mean Squared Error) and Bias of EKE for each OGCM model vs EKE from AVISO data. Grey shaded show the OGCM with better characteristic according to values of metrics validations.

| **Statistic parameters** | **ECCO** | **SODA** | **HYCOM** | **Mercator** |
|---|---|---|---|---|
| MAE | 0.0078 | 0.0072 | 0.0072 | 0.0064 |
| RMSE | 0.0101 | 0.0102 | 0.0123 | 0.0085 |
| BIAS | -0.0078 | -0.0015 | 0.0008 | 0.0029 |

Table 4: Validations made over temporals means for the whole area of NEA between the three ROMS experiments and SST satellite data from AVHRR and MW_SST.

| Exp. | RMSE | | Bias | | Corr. Coef. | |
|---|---|---|---|---|---|---|
| | AVHRR | MW_SST | AVHRR | MW_SST | AVHRR | MW_SST |
| R_M | 0.43 | 0.48 | 0.43 | 0.48 | 0.99 | 0.99 |
| R_NQ | 0.63 | 0.70 | 0.61 | 0.67 | 0.99 | 0.99 |
| R_C | 0.66 | 0.67 | -0.05 | 0.004 | 0.96 | 0.96 |